Aerospace Science and Technology 120 (2022) 107260

Contents lists available at ScienceDirect

Aerospace Science and Technology

www.elsevier.com/locate/aescte

A coaxial quadrotor flying robot: Design, analysis and control implementation

S. Jamal Haddadi [a], P. Zarafshan [b,*], M. Dehghani [c]

[a] Department of Electrical and Automation Systems, University of Federal de Santa Catarina, Florianopolis, Brazil
[b] Department of Agro-Technology, College of Aburaihan, University of Tehran, Tehran, Iran
[c] Department of Food Technology, College of Aburaihan, University of Tehran, Tehran, Iran

ARTICLE INFO

Article history:
Received 16 April 2021
Received in revised form 12 October 2021
Accepted 29 November 2021
Available online 1 December 2021
Communicated by Tsourdos Antonios

Keywords:
Octorotor
Dynamics
Control
Fuzzy-PID controller
Disturbance

ABSTRACT

In this paper, the analysis, design and fabrication of an Octorotor Miniature Aerial Vehicle (MAV) are presented. This rotorcraft setup can act as an autonomous robot in outdoor environments to carry and move high payloads, and can thus also be used in object manipulation tasks. Within this paper, the system design, dynamic modeling, control system design, and its implementation are elaborated. The design procedure for this MAV includes two mechanics and electronics sub systems, which are thoroughly discussed. The mechanical design covers the aerodynamics analysis, body components, and propulsion system implementation. The electronic design includes hardware selection and control system design for the presented aerial robot. Since the MAV flies in outdoor environments, it additionally has to cope with windy conditions. Hence, the stabilization control scheme is considered along the lines of usual PID controllers. The attitude controller, as well as the inner and outer control loops, are fully studied, and a Fuzzy-PID controller is developed to improve the performance. Finally, considering maneuvers in two case studies, simulation and implementation results are studied and compared.

1. Introduction

In the last years, multi-rotors design, control and implementation are challenges which has become prevalent by researchers, [1,2]. Multi-rotors are robust helicopters whereas they do not have the complicated swash-plates and linkages found in the conventional rotorcraft, [3]. The main restrictions on the use of helicopters made us use flying robots which have low weight and less cost and more secure flights. In this regard, Unmanned Aerial Vehicles (UAVs) are used for different purposes such as traffic monitoring, patrolling for forest fires, surveillance, landslide and rescue missions, with no pilot risks, independently or in cooperation with other robotic systems, [4–6]. UAVs can be also used in indoor and outdoor applications. One kind of these UAVs that can be used in the mentioned applications are Quadrotor. Quadrotors are placed in Micro Aerial Vehicle (MAV) families. MAVs can be operated on a wide area regardless of the effect of ground configuration. An X4-Rotor UAV has been conceived by a team from the Australian National University to use as a highly-reliable experimental platform, [7]. The merit of MAVs is maximized for practical use in the places where it is dangerous and difficult to access. Furthermore, MAVs are greatly cheaper and safer in dangerous tasks rather than piloted aircraft. In [8,9], the authors attempt to build a fully operational and open-source Quadrotor with a moderate cost. Other experimental flying platforms with vertical take-off and landing capabilities are studied in [10,11]. The full design of a Quadrotor as a platform for monitoring indoor environments is also presented in [12]. If small size is the key factor, the best choice among UAVs is multi-rotors.

A coaxial Octorotor uses four arms, with eight motors in which a couple of motors are coaxially placed up and down at the end of each arm. Certainly, when the number of motors in MAVs is increased, this configuration is expected to generate more thrust for the vehicle, besides more robustness against rotor failures. Also, the number of rotating propellers is expected to give more stability, since the coaxial configuration cancels the torque of one another. In [13], an adaptive multiple actuator fault tolerant formation control for Octorotors is presented. In [14], a Hexarotor robot is proposed and its tolerance against any propeller failure is proved.

The dynamic model of such robots can be described as a set of ordinary differential equations, which are usually nonlinear and

* Corresponding author.
E-mail address: p.zarafshan@ut.ac.ir (P. Zarafshan).

https://doi.org/10.1016/j.ast.2021.107260
1270-9638/

coupled, [15]. Through analyses have been presented on the dynamic modeling and analysis, [16,17]. Moreover, control of these flying systems currently is an ongoing research subject because of its applications, [18–20]. Multirotor robots are considered as underactuated systems with nonlinear dynamics, which brought challenges in control designs, [21]. In [22], a control algorithm is proposed for precise trajectory tracking under windy environments, using acceleration error feedback. In [23], a robust fuzzy controller for attitude control of a quadrotor is developed, using Takagi-Sugeno fuzzy model for dynamics nonlinearities. In [24], a fixed-time sliding mode observer based control is presented for safety against disturbances and actuator faults. Besides control concerns, optimization is another important challenge due to energy limitations of batteries, which requires proper trajectory design and control based on the dynamics of the system, [25]. Disturbance rejection [26], optimal control [27] and adaptive control [28] have been widely considered. Besides very advanced and robust controllers, the investigation of open source and commercial robots reveals that Proportional Integral Derivative (PID) controllers are used with success. In [29], a PID controller and a Linear Quadratic Regulator (LQR) are implemented and compared. Typically, these PID controllers are applied to a linearized dynamic model of the aerial vehicle. The controllers effectively attain the system stability if the vehicle is in a configuration near the point in which the model is linearized. However, the performance dramatically declines if the vehicle state significantly differs from this desired equilibrium, [30].

In this paper, design, fabrication, dynamics and trajectory tracking controller design and implementation for an autonomous Octorotor flying robot are presented. In section 2, the mechanical design is introduced. Section 3 presents the robot dynamics. The electronics design and parts of the robot are introduced in section 4. Then, in section 5 a Fuzzy PID controller is designed to keep robot attitude and altitude in control even in presence of wind disturbances. Finally, simulation and experimental results of our manufactured robots are presented and discussed in section 6. The main contributions of this work can be highlighted as manufacturing the Octorotor in order to increase the payload capacity and the degree of actuation, without increasing its size; and, developing a fuzzy PID controller for the Octorotor stability in windy conditions, with simple controller design and calculations.

2. Mechanical design of Octorotor

The structure of the proposed eight-rotor UAV has a square cross body, made of four arms with identical lengths. At the end of each arm, tow force generating motors are mounted to produce the required control forces/torques. Each arm is made of a carbon fiber hollow rod, with a length of 17 cm, and with circular cross-section of 13 mm outer diameter and 11 mm inner diameter. In these rods, specific carbon fiber components are exploited to provide a superior torsional/shear strength to weight ratio, produced in a special sheet winding composite materials fabrication process, [31]. The mechanics of the Octorotor frame is depicted in Fig. 1.

To fix the carbon fiber pipes in between the two chassis plates, polyamide parts are used as depicted in the figure. For the electronic boards and equipment, a third plate is placed on the chassis, mounted on rubber dampers, in order to damp the motor vibrations that travel to the chassis through the arms. Two sets of motors and propellers are installed on each arm of the Octorotor, as the actuation units. As depicted, the propellers of each unit are coaxial. This design can increase thrust force and maneuverability without increasing the robot width. To drive the propellers, Brushless Direct Current (BLDC) motors are used. The motor rotor and stator and its three wire connectors are depicted in the figure. Using an Electronic Speed Control (ESC) unit, the motor speed is controlled, while the motor feedback is sent back to the controller, through the wires. Each motor rotates a propeller, as depicted. The robot propellers have a diameter of 8 inches. The propellers are mounted directly on the motors, without any coupling or speed reduction system.

3. Dynamic modeling of Octorotor

The dynamics model of the Octorotor must be derived for model-based controller introduced in next sections. The flight kinematics of the robot is illustrated in Fig. 2. Since the propellers are mounted as coaxial pairs, the kinematics and dynamics of this robot is very similar to those of the Quadrotors, [32]. The motors are numbered as depicted. The rotary speeds of the motors are determined by ω_1 to ω_8 respectively to the numbers in the figure. The robot has 6 degrees of freedom, as expected, which are represented by x, y and z linear coordinates and the standard Roll, Pitch and Yaw angles.

Considering the gyroscopic effects, gravitation and Octorotor inertia, then motion can be modeled. In fact, by considering the flight theory of Octorotor, its motion equations are the same as the motion equations of quadrotors. It should be noted that an inertia frame must be used as a universal reference frame in the dynamic analysis of robotic systems which is also considered for this robot. In this section, Newton-Euler equations of motion are used for dynamic modeling of the Octorotor. For this approach, and also for control applications, the Octorotor motion is determined both according to the Octorotor coordinates depicted in the figure, and also according to an inertial frame on the ground. Here, the position vector of the Octorotor is denoted by $\mathbf{p} = [x, y, z]^T$, and its vector of angular velocity is represented by $\boldsymbol{\omega} = [\omega_x, \omega_y, \omega_z]^T$. To transform these vectors between the inertial and moving frames, we have

$$\boldsymbol{\omega}_{\mathrm{E}} = \mathbf{R}\boldsymbol{\omega}_{\mathrm{B}} \tag{1}$$

$$\dot{\boldsymbol{\Omega}} = \mathbf{T}\boldsymbol{\omega}_{\mathrm{B}} \tag{2}$$

where, Ω_{E} is the angular velocity vector in the inertial frame; Ω_{E} is the angular velocity vector in the body-fixed frame; $\mathbf{R}$ is the rotation matrix; $\mathbf{T}$ is the transfer matrix between Euler derivatives and the angular velocity vector; $\boldsymbol{\Omega}$ represents the orientation, using the Yaw, Pitch and Roll angles as the Euler angles for rotation about z, y and x axes respectively. Hence, the Octorotor orientation is represented by

$$\boldsymbol{\Omega} = \begin{bmatrix} \varphi & \theta & \psi \end{bmatrix}^T \tag{3}$$

where, φ, θ and ψ are Roll, Pitch and Yaw angles respectively, [33]. Then, the rotation matrix $\mathbf{R}$ and the transfer matrix $\mathbf{T}$ are determined as:

$$\mathbf{R} = \begin{pmatrix} \mathrm{c}\theta\mathrm{c}\psi & \mathrm{s}\varphi\mathrm{s}\theta\mathrm{c}\psi - \mathrm{c}\varphi\mathrm{s}\psi & \mathrm{s}\varphi\mathrm{s}\psi + \mathrm{c}\varphi\mathrm{s}\theta\mathrm{c}\psi \\ \mathrm{c}\theta\mathrm{s}\psi & \mathrm{s}\varphi\mathrm{s}\theta\mathrm{s}\psi + \mathrm{c}\varphi\mathrm{c}\psi & \mathrm{c}\varphi\mathrm{s}\theta\mathrm{s}\psi - \mathrm{s}\varphi\mathrm{c}\psi \\ -\mathrm{s}\theta & \mathrm{s}\varphi\mathrm{c}\theta & \mathrm{c}\varphi\mathrm{c}\theta \end{pmatrix} \tag{4}$$

$$\mathbf{T} = \begin{pmatrix} 1 & \mathrm{s}\varphi\mathrm{t}\theta & \mathrm{c}\varphi\mathrm{t}\theta \\ 0 & \mathrm{c}\varphi & -\mathrm{s}\varphi \\ 0 & \mathrm{s}\varphi\mathrm{c}\theta & \mathrm{c}\varphi\mathrm{c}\theta \end{pmatrix} \tag{5}$$

where c, s and t represent cos(), sin() and tan() functions, respectively.

Fig. 1. Mechanics of the Octorotor robot; (a) the robot; (b) chassis plates; (c) polyamide parts to connect rods; (d) the actuation unit on each arm; (e) two installed motors on each actuation unit; (f) the Brushless Direct Current motors (BLDC); (g) the propeller; (h) the board vibration dampers.

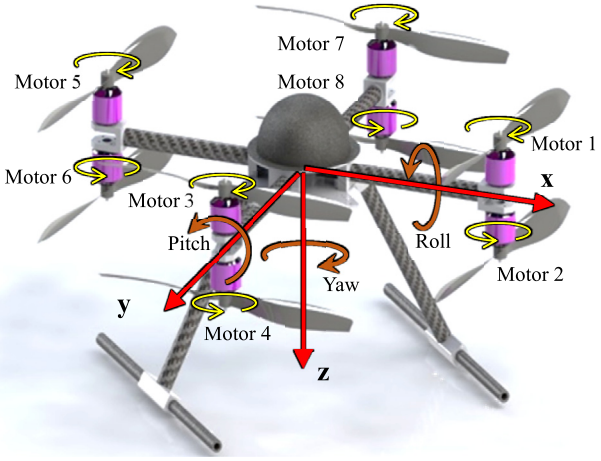

Fig. 2. Flight kinematics of the Octorotor.

The robot velocity, represented in the body frame, is $\mathbf{V}_B$. Then, $\mathbf{a}_B$, the acceleration of the Octorotor, with respect to the inertial frame, expressed in the body frame, is

$$\mathbf{a}_B = \dot{\mathbf{v}}_B + \boldsymbol{\omega}_B \times \mathbf{v}_B \tag{6}$$

Hence, using the Newton-Euler equations, the dynamics of motion of the Octorotor can be described as:

$$\begin{cases} m(\dot{\mathbf{v}}_B + \boldsymbol{\omega}_B \times \mathbf{v}_B) = \mathbf{F}_B \\ \mathbf{I}\dot{\boldsymbol{\omega}}_B + \boldsymbol{\omega}_B \times (\mathbf{I}\boldsymbol{\omega}_B) = \boldsymbol{\tau}_B \end{cases} \tag{7}$$

where, m is the Octorotor mass; $\mathbf{I}$ is the matrix of inertia expressed in the body frame; $\mathbf{F}_B$ and $\boldsymbol{\tau}_B$ are sums of all applied forces and torques, respectively, expressed in the body frame. These forces and torques consist of gravitation, propeller effects, air and wind drag, etc. Since the mass distribution of Octorotor is symmetrical, the inertia matrix is diagonal. For our hover flight application, the above dynamic model can be simplified for all its 6 dimensions, expressed by x, y and z positions, and roll, pitch and yaw angles. Hence, replacing $\boldsymbol{\omega}$ by $\boldsymbol{\Omega}$ and using (1) to (5), and representing the wind disturbance on the by D, and substituting the dynamic forces and torques of the propellers, the translational and rotational dynamics of Octorotor are obtained as:

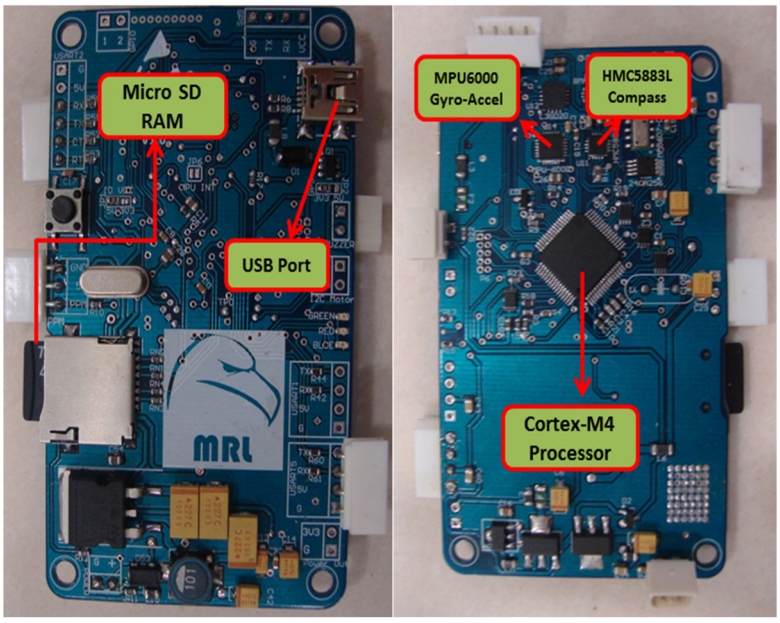

Fig. 3. The designed electronic board.

$$\begin{cases} \ddot{\varphi} = \left(\dfrac{I_y - I_z}{I_x}\right)\dot{\theta}\dot{\psi} + \dfrac{J_{TP}}{I_x}\dot{\theta}\omega_r + \dfrac{U_2}{I_x} \\ \ddot{\theta} = \left(\dfrac{I_z - I_x}{I_y}\right)\dot{\psi}\dot{\varphi} - \dfrac{J_{TP}}{I_y}\dot{\varphi}\omega_r + \dfrac{U_3}{I_y} \\ \ddot{\psi} = \left(\dfrac{I_x - I_y}{I_z}\right)\dot{\varphi}\dot{\theta} + \dfrac{U_4}{I_z} \\ \ddot{x} = \dfrac{1}{m}\left(c\varphi s\theta c\psi + s\psi s\varphi\right)U_1 + \dfrac{D_x}{m} \\ \ddot{y} = \dfrac{1}{m}\left(c\varphi s\theta s\psi - s\varphi c\psi\right)U_1 + \dfrac{D_y}{m} \\ \ddot{z} = \dfrac{1}{m}\left(c\theta c\varphi\right)U_1 - g + \dfrac{D_z}{m} \end{cases} \tag{8}$$

where, J_{TP} is the total rotational inertia around the propeller axis, and g is the constant of gravitational acceleration. Furthermore, ω_r is the total speed or propeller's residual speed, defined as:

$$\omega_r = -\omega_1 + \omega_2 - \omega_3 + \omega_4 - \omega_5 + \omega_6 - \omega_7 + \omega_8 \tag{9}$$

In addition, system input components U_1, U_2, U_3, U_4 are defined as:

$$\begin{aligned} U_1 &= b\left(\omega_1^2 + \omega_2^2 + \omega_3^2 + \omega_4^2 + \omega_5^2 + \omega_6^2 + \omega_7^2 + \omega_8^2\right) \\ U_2 &= lb\left(-\omega_3^2 - \omega_4^2 + \omega_7^2 + \omega_8^2\right) \\ U_3 &= lb\left(-\omega_5^2 - \omega_6^2 + \omega_1^2 + \omega_1^2\right) \\ U_4 &= d\left(-\omega_1^2 + \omega_2^2 - \omega_3^2 + \omega_4^2 - \omega_5^2 + \omega_6^2 - \omega_7^2 + \omega_8^2\right) \end{aligned} \tag{10}$$

where, ω_i is the angular velocity of the i^{th} propeller; b is the thrust factor; and d is the drag factor. Since the BLDC motors are located at the end of bars, l is the length from the body center to the motors, [29]. This presented model considers the full dynamics of the Octorotor flying robot, regardless of the actuator dynamics. However, the dynamic performance of motors is one of the most important factors in a robot dynamics, specifically when the system reaction is very fast. The interactions between the dynamics of the BLDC motors with the air can be attained as:

$$\dot{\omega}_n = -\frac{K_E K_M}{R J_{TP}}\omega_n - \frac{d}{J_{TP}}\omega_n^2 + \frac{K_M}{R J_{TP}}\upsilon_n \tag{11}$$

where, ω_n is the angular velocity of BLDC motor; υ_n is the applied voltage to the motor connectors; and, the other parameters are constant coefficients of the motor and its power transmission system.

4. Electronics and hardware design

The flight control data are monitored by Mission Planner software. Besides, the flight data are saved in a micro SD memory, which is installed on the electronic board. Then, the saved data are converted to a MATLAB file. After the flight, these data are sent to MATLAB/SIMULINK software. In order to process the data, an ARM Cortex M4 processor is used, as the main controller on the Octorotor. This board is also equipped with an MPU6000 gyro-acc sensor, that exploits a 3-axis gyroscope and a 3-axis accelerometer on the same silicon die together. This gyro-acc sensor has an onboard Digital Motion Processor (DMP) with the capability to process complex 9-axis motion fusion algorithms. Moreover, there is an HMC5883L compass on the Quadrotor to determine the direction changes.

The robot processor works with other parts, including a 7-channels 2.4 GHz RX R710 DSM2 receiver, eight Pentium 30A ESC drivers, eight BLDC motors, and an 11.1 Volt 2.2A battery, which are all mounted on the Octorotor. The controller receives inputs of the Octorotor from the RX R710 DSM2 receiver. The designed electronic board is shown in Fig. 3. The RX R710 DSM2 receiver generates PWM signals and the MPU6000 sensor generates data as digital inputs. These data are applied to the slave processor, and the slave processor gives all the data to the master processor, via a universal asynchronous receive/transmit (UART) bus. These data transfer through the TX port of the slave processor to the RX port of the master processor. When the Octorotor flies to the desired area, the gyro-acc sensor helps automatically stabilize the Octorotor, while the PWM output affects the stabilization of the Octorotor system. For the attitude control, all the data is taken

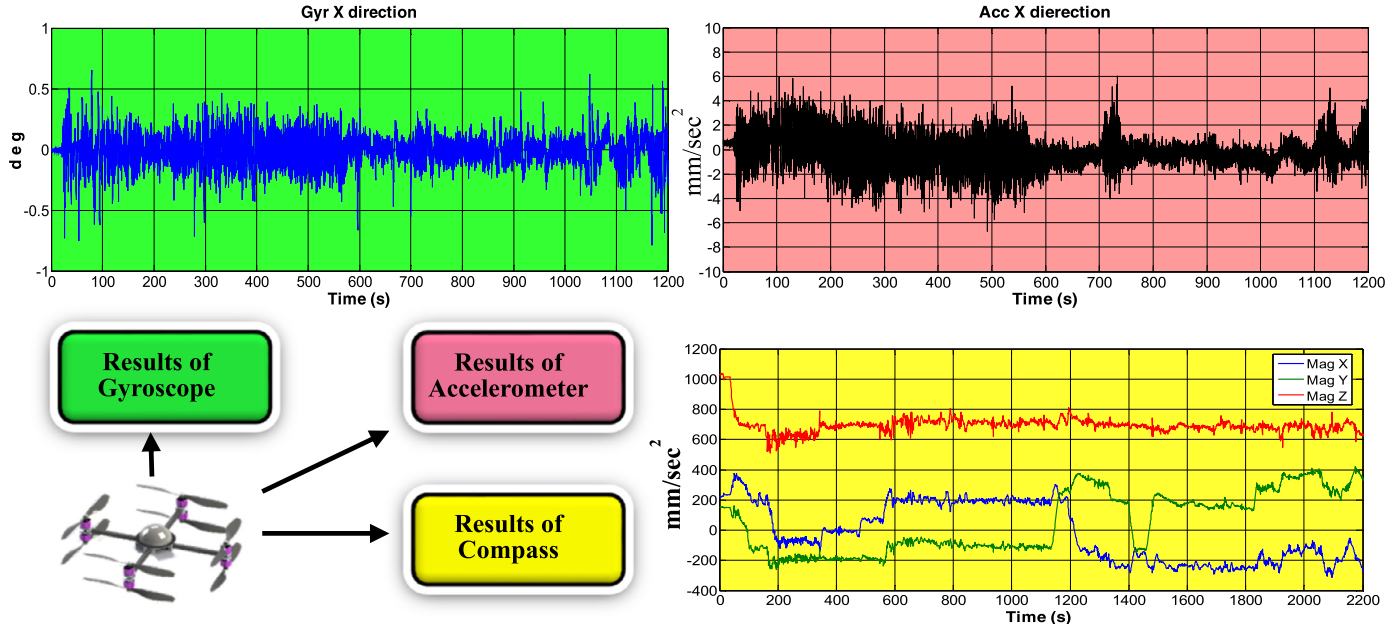

Fig. 4. IMU results from an experimental test. (For interpretation of the colors in the figure(s), the reader is referred to the web version of this article.)

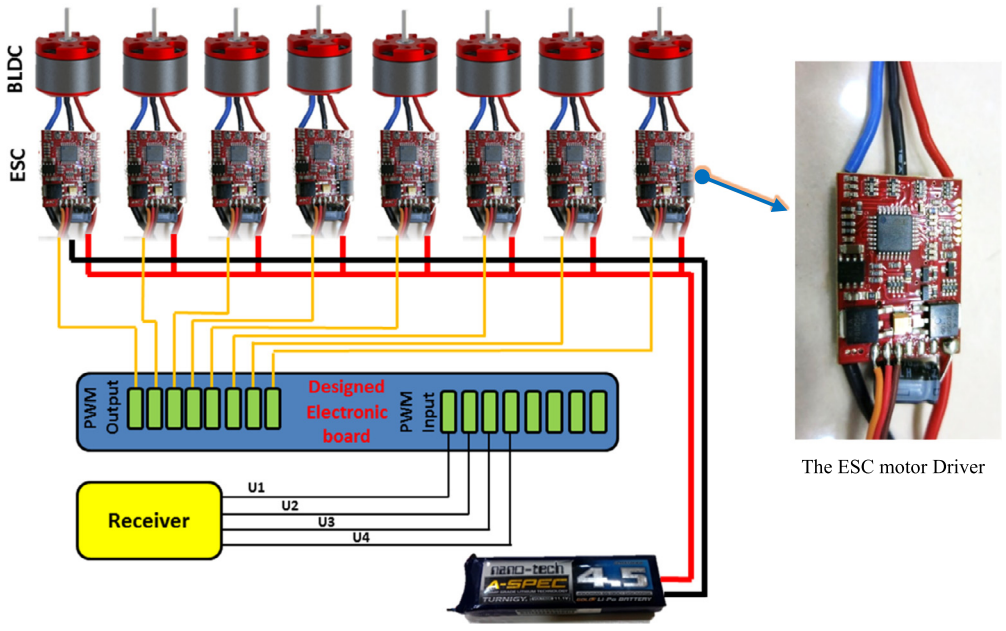

Fig. 5. Controller hardware architecture.

from the IMU (Inertial Measurement Unit), with the 100 Hz frequency. Some results of the IMU measurements of an experimental study are depicted in Fig. 4. Furthermore, to effectually drive the eight BLDC motors, I2C speed controllers are selected. Moreover, an HMTR module with 414 MHz wireless data is used to communicate between the ground station and the flying robot. This designed hardware architecture of the flight control system is depicted in Fig. 5.

As mentioned, the BLDC motors are controlled through the specific BLDC motor drivers. The motor driver that is used is a 30A ESC Pentium as shown in the figure. The PWM signals are sent to this motor driver as its control input. This signal is produced and sent from the ATMega2560 processor, based on the remote control, and the sensors. This driver can drive motors up to 30A, which is greater than the requirements of the Octorotor BLDC motors.

5. Control system design

In this section, the proposed controller is introduced in detail. This controller consists of an inner control loop and an outer control loop. In general, PID-based attitude control structures have been widely demonstrated for a variety of multi-rotor aircraft configurations [21], and other more or less similar systems, [34,35]. Here, the designed Octorotor controller is modified by a fuzzy inference system, so that the controller gains are tuned to achieve better responses and less errors. As mentioned before, four control inputs are defined for the 6-DOF Octorotor. From this point of view, the robot can be considered to be under-actuated. Hence, it should be controlled using a closed-loop controller, to ensure its stability in following a given trajectory. The proposed controller consists of two loops which are introduced below.

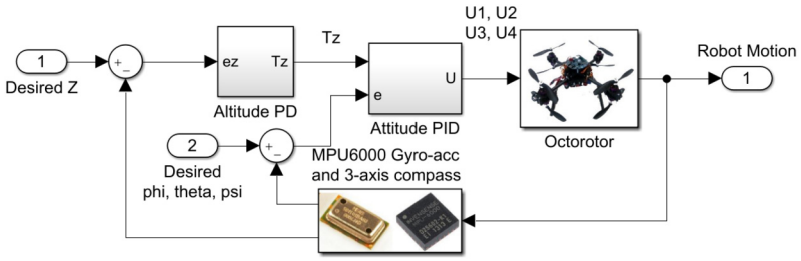

Fig. 6. The cascade controller.

5.1. PID controller

5.1.1. The inner control loop

The Octorotor has three DOFs for the rotational movements and three DOFs for the translation movements. As seen in (7) and (8), the rotational motion does not depend on the translational motion while the opposite is not true. Thus, the cascade control architecture is chosen for the attitude and position control of the flying robot, as depicted in Fig. 6. The inner control loop is designed for the stability. Therefore, it is an attitude controller that controls the Euler angles of the system. The outer control loop is considered for regulating the robot altitude. Hence, it is responsible for the slower dynamics. The main control structure of the Octorotor is almost similar to its equivalent quadrotor, [36,37]. However, the eight rotors provide actuation redundancy. Here, this redundancy is resolved by choosing equal speeds for each couple of coaxial rotors, as the default choice.

To stabilize roll, pitch and yaw angles, attitude control contains three separate PID controllers to keep system states at the desired equilibrium point. Thus, the control law can be described as:

$$\mathbf{U} = \mathbf{K_p e}\,(t) + \mathbf{K_i}\int_0^t \mathbf{e}\,(\tau)\,d\tau + \mathbf{K_d}\frac{d\mathbf{e}\,(t)}{dt} \tag{12}$$

where $\mathbf{K_p}, \mathbf{K_i}, \mathbf{K_d}$ are the controller gains; $\mathbf{e}$ is the error signal defined as the difference between the desired values of attitude angles and the measured values obtained by the sensors at each time step, defined as:

$$\begin{aligned} e_\varphi\,(t) &= \varphi_d\,(t) - \varphi\,(t) \\ e_\theta\,(t) &= \theta_d\,(t) - \theta\,(t) \\ e_\psi\,(t) &= \psi_d\,(t) - \psi\,(t) \end{aligned} \tag{13}$$

Based on (12) and (13), and reminding that the gain matrices are diagonal, the PID controller reduces the errors based on the following equations:

$$\begin{aligned} U_2 &= K_{p\varphi} e_\varphi\,(t) + K_{i\varphi}\int_0^t e_\varphi\,(\tau)\,d\tau + K_{d\varphi}\frac{de_\varphi\,(t)}{dt} \\ U_3 &= K_{p\theta} e_\theta\,(t) + K_{i\theta}\int_0^t e_\theta\,(\tau)\,d\tau + K_{d\theta}\frac{de_\theta\,(t)}{dt} \\ U_4 &= K_{p\psi} e_\psi\,(t) + K_{i\psi}\int_0^t e_\psi\,(\tau)\,d\tau + K_{d\psi}\frac{de_\psi\,(t)}{dt} \end{aligned} \tag{14}$$

5.1.2. The outer control loop

The altitude control is designed as an outer loop to keep the height in a desired position of the z-axis. Since its lower priority from the attitude control, the height control is designed as the second control loop with the simple PD control law as:

$$\begin{aligned} T_z &= k_p\,(z_d - z) + k_d\,(\dot{z}_d - \dot{z}) - mg \\ T &= -T_z / c\varphi c\theta \end{aligned} \tag{15}$$

where T is the magnitude of the thrust force; and T_z is its vertical component. Thus, the altitude control law can be presented:

$$U_1 = -\frac{1}{c\varphi c\theta}\left(k_p\,(z_d - z) + k_d\,(\dot{z}_d - \dot{z}) - mg\right) \tag{16}$$

5.2. Fuzzy controller

The most important challenge for the Octorotor control, is to keep it stable in presence of wind disturbances. A PID controller, as discussed in the previous section, could provide a good performance. However, in presence of disturbances, the controller can be improved. In this section, a Fuzzy-PID system is introduced, which is chosen for the Octorotor control. In this system, the PID control coefficients are determined in real time, using a fuzzy system. In general, this nonlinear controller has the potential to provide better performance in a nonlinear system, provided the coefficients are properly tuned. Firstly, the PID coefficients from the previous section are chosen. Then, using fuzzy rules, and based on expert's opinion and experimental tests, the coefficients are regulated. As an instance for the proportional coefficient $k_{p\varphi}$ for the φ angle, the online regulation is as follows

$$K_{p\varphi,\text{regulated}} = K_{p\varphi,\text{PID}} + K_{p\varphi,\text{fuzzy}} \times \text{FIS}(e_\varphi, \dot{e}_\varphi) \tag{17}$$

where, $k_{p\varphi,\text{regulated}}$ is the newly updated proportional coefficient; $k_{p\varphi,\text{PID}}$ is the PID coefficient from the previous section; $k_{p\varphi,\text{fuzzy}}$ is a constant coefficient for the fuzzy regulation; and FIS() is a factor to be multiplied by $k_{p\varphi,\text{fuzzy}}$, determined by the fuzzy inference system, based on a look up table for the error e_φ and its derivative. A diagram of the fuzzy inference system is depicted in Fig. 7. As an example for φ angle, the membership functions and the fuzzy system surface for k_p factor of (17) are shown. The same equations are used for all other controller coefficients. This controller diagram is depicted in Fig. 8.

In order to tune the fuzzy membership functions and the fuzzy rules, simulation and experimental tests by an expert was required. The controller was supposed to keep the robot in a desired condition, even in the presence of disturbances. In order to tune the fuzzy parameters, after simulations, we designed a setup to apply wind disturbance and observe the performance, while the fuzzy coefficients were tuned by an expert pilot, online. The coefficients were changed, until the errors became minimum. The same process was carried out in outdoor experiments, using wireless connection between the Octorotor controller and the station computer, for online observation and tuning. Finally, the tuned Fuzzy-PID controller provides better performance, compared to the classical PID controller. The experimental setup and a comparison of the results are depicted in Fig. 9.

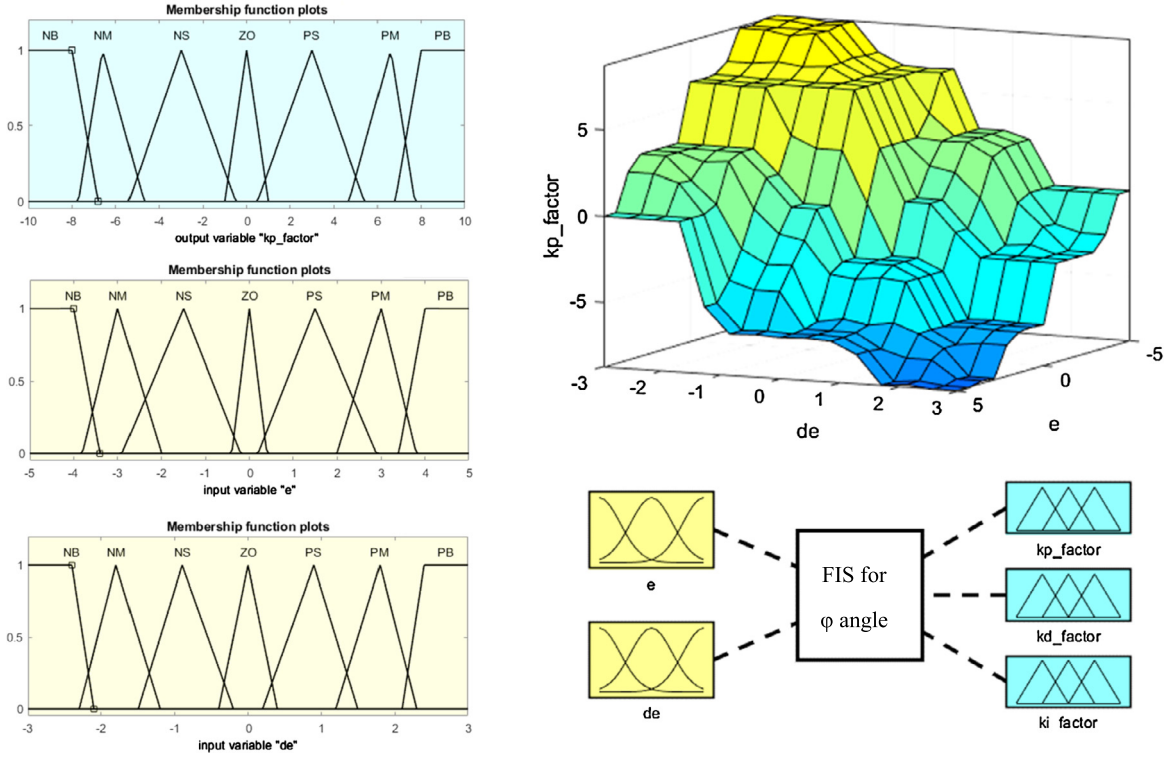

Fig. 7. The fuzzy inference system. (Left) membership functions; (Right Up) fuzzy surface of k_p factor; (Right Down) the fuzzy inference system.

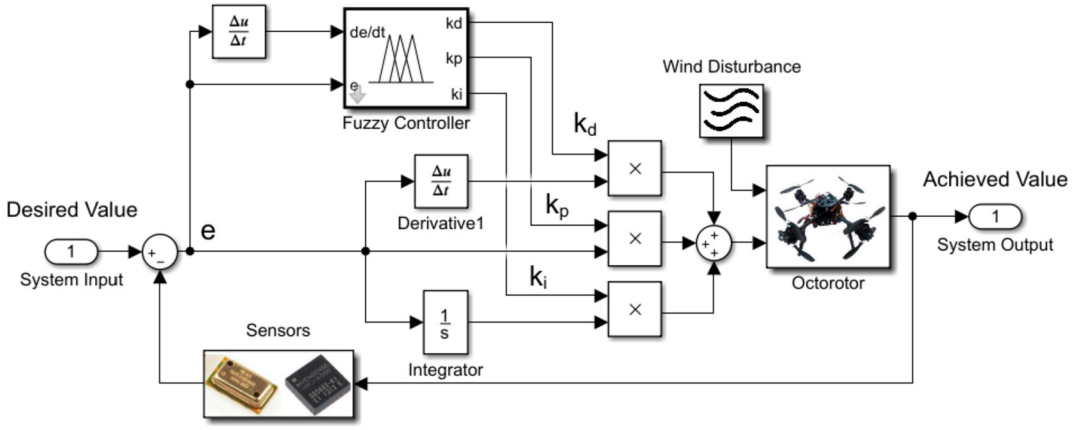

Fig. 8. Diagram of the fuzzy controller.

6. Obtained results and discussions

In this section, the proposed control strategy is performed and tested by both, software simulation and experimental tests. The initial simulations by MATLAB/SIMULINK were helpful in designing and tuning controllers, before experiments. Secondly, real experimental results of the Octorotor flight are presented. Besides the robot results, the flight environment in which the robot flies are introduced. This robot has been manufactured by our team at Mechatronics Research Lab (MRL) in Qazvin Islamic Azad University.

6.1. Simulation results

For the simulations, the properties of the real Octorotor are considered. The main parameters of the Octorotor, used in simulations, are listed in Table 1.

Table 1
Parameters of the designed Octorotor.

Parameters	Description	Value	Unit
m	Mass	1.375	Kg
l	Octorotor arm length	0.195	m
I_x	Inertia on x axis	0.006228	Kg·m^2
I_y	Inertia on y axis	0.006228	Kg·m^2
I_z	Inertia on z axis	0.01125	Kg·m^2
J_{TP}	Transpose Inertia	154×10^{-7}	Kg·m^2
d	Drag factor	2.9842×10^{-5}	–
b	Thrust factor	3.2320×10^{-5}	–

The proposed control strategy is implemented in MATLAB/SIMULINK simulations. The achieved results for orientation control are shown in Fig. 10. The controller successfully regulates motor speeds and overcomes the measurement noises and wind disturbances. As depicted in the diagrams, yaw angle changes more

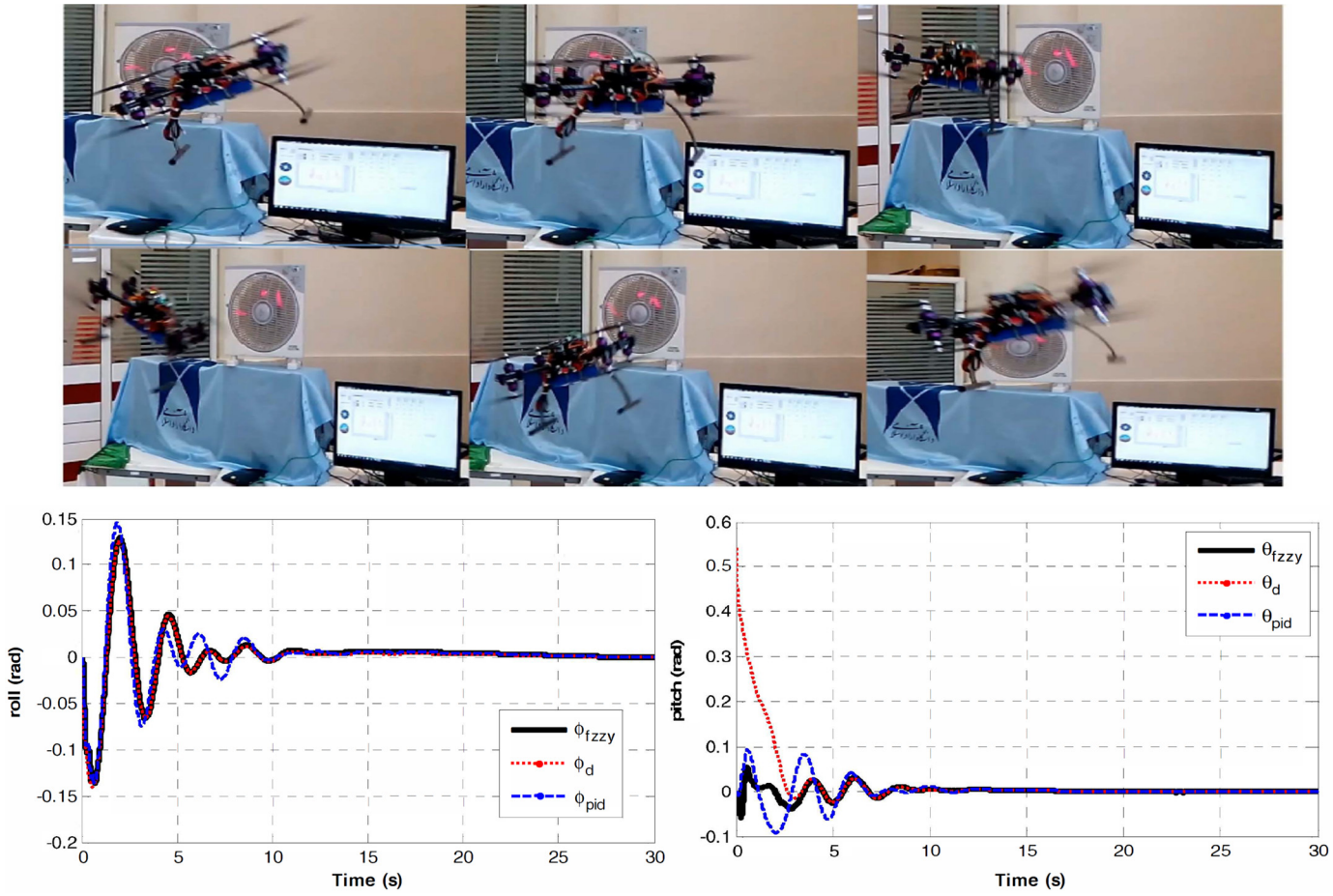

Fig. 9. Performance of the fuzzy controller and the setup for its tuning.

slowly than pitch and roll angles, due to the system dynamics and the controller structure. As a comparison, the achieved rms (root mean square) error of the Roll angle using the developed fuzzy controller is 0.026, while using the classical PID controller this error is 0.112.

Similarly, the implemented altitude controller regulates the Octorotor position to its desired set-point in 2 seconds, as shown in Fig. 11. It is observed that the Octorotor maintains its height in 25 m, even in the presence of the sensor noises. The figure also shows the results for trajectory control. The robot starts motion from an initial position which is lower than the desired altitude. After 2 seconds, the Octorotor reaches the desired height and follows the reference trajectory. The achieved trajectory shows that the controller can regulate motor speeds and stabilize the Octorotor, while the desired maneuverability is achieved.

6.2. Experimental results

To study the performance of the designed PID controller, two trajectories are considered in two case studies. In case study I, the Octorotor autonomously takes off and tracks a square path around a building on the campus. In case study II, the Octorotor moves a 500 m distance between two buildings. These paths are shown in Fig. 12. Subsequently, the experimental results of the Octorotor for these two cases are presented.

Case Study I: It should be noted that the environment where the experiments were performed is a 500-m long and 350-m width area. The Octorotor follows a path as shown in Fig. 12-a. The Octorotor follows a square path at the 25 m height but its height reduces to 20 m due to land slope. Finally, it comes back to the predetermined point. This experiment was carried out in an environment where there was a little wind.

Case Study II: The altitude of this case study is 50 m, which is twice the altitude in case study I. This altitude is chosen because in this height, air is windier and consequently the Octorotor flies with more difficulties. As the previous case, the robot automatically takes off from the start point and comes automatically back to the first place. Fig. 12-b shows the selected path in the mission map. The achieved maneuver path of the Octorotor in the two experiments is shown in Fig. 13.

The performance of the controller is depicted in Fig. 14, using the track of the desired and the achieved Euler angles of the Octorotor. As shown in this figure, there are similar performances for roll and pitch angles. Comparing the diagrams, the effect of more wind in the second case is obvious. Furthermore, the desired and achieved velocities determined by the IMU are shown in Fig. 15. The measured rms error for position in the first case study is 1.32 m, and in the second case study is 0.88 m, noting different path and environmental conditions.

7. Conclusions

In this paper, the design, modeling and control of an Octorotor with coaxial motors was studied. The Octorotor would be able to work as an autonomous flying robot in outdoor environments. The robot design was introduced in two separate mechanical and electrical sections. Robot dynamic model was introduced, as used for the control purposes. In the electronic design section, the design of the electronic board and parts were introduced. To attain

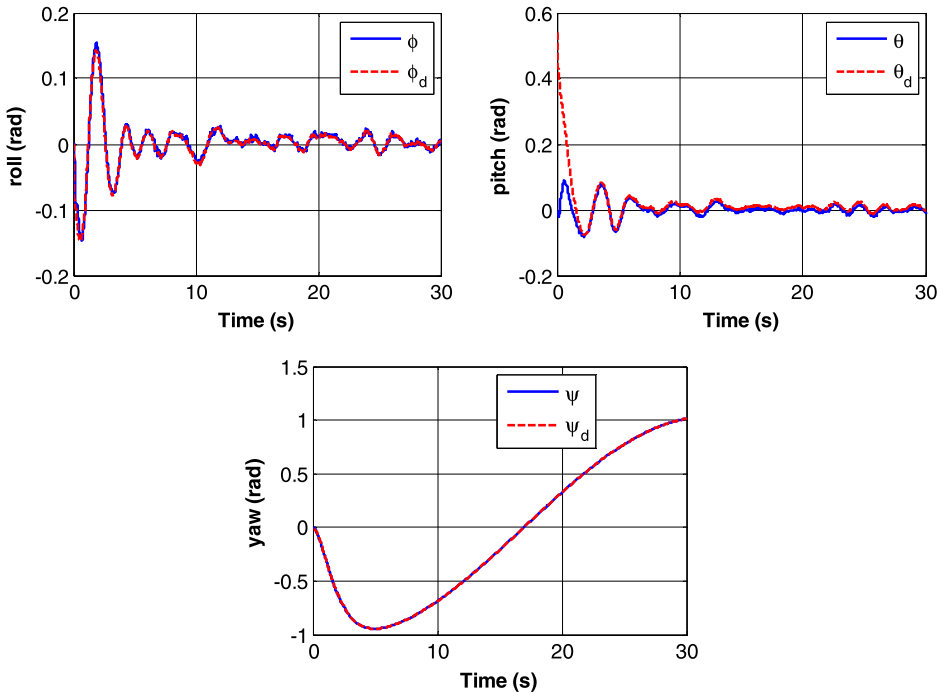

Fig. 10. Octorotor attitude using the designed PID controller in simulation.

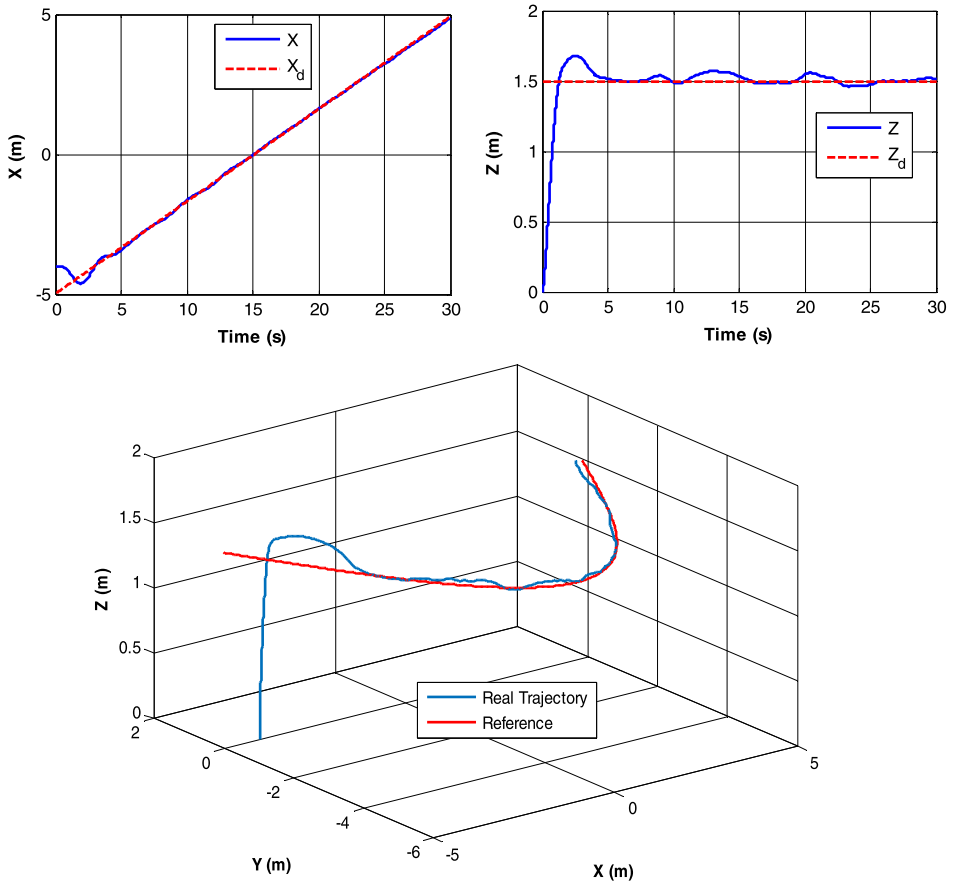

Fig. 11. The results of the Octorotor trajectory control.

a successful maneuver by this flying robot and with the calculation power of ordinary microprocessors, a fuzzy-PID controller was designed and applied. This controller was used to control the robot in presence of wind disturbances. The fuzzy inference system was regulated using simulations and experimental tests. Finally, to study the performance of the designed flying robot, two outdoor experimental testes were carried out. The results showed the successful performance of the robot and its control system. Compared

a) Case study I b) Case study II

Fig. 12. Determined paths for robot motion.

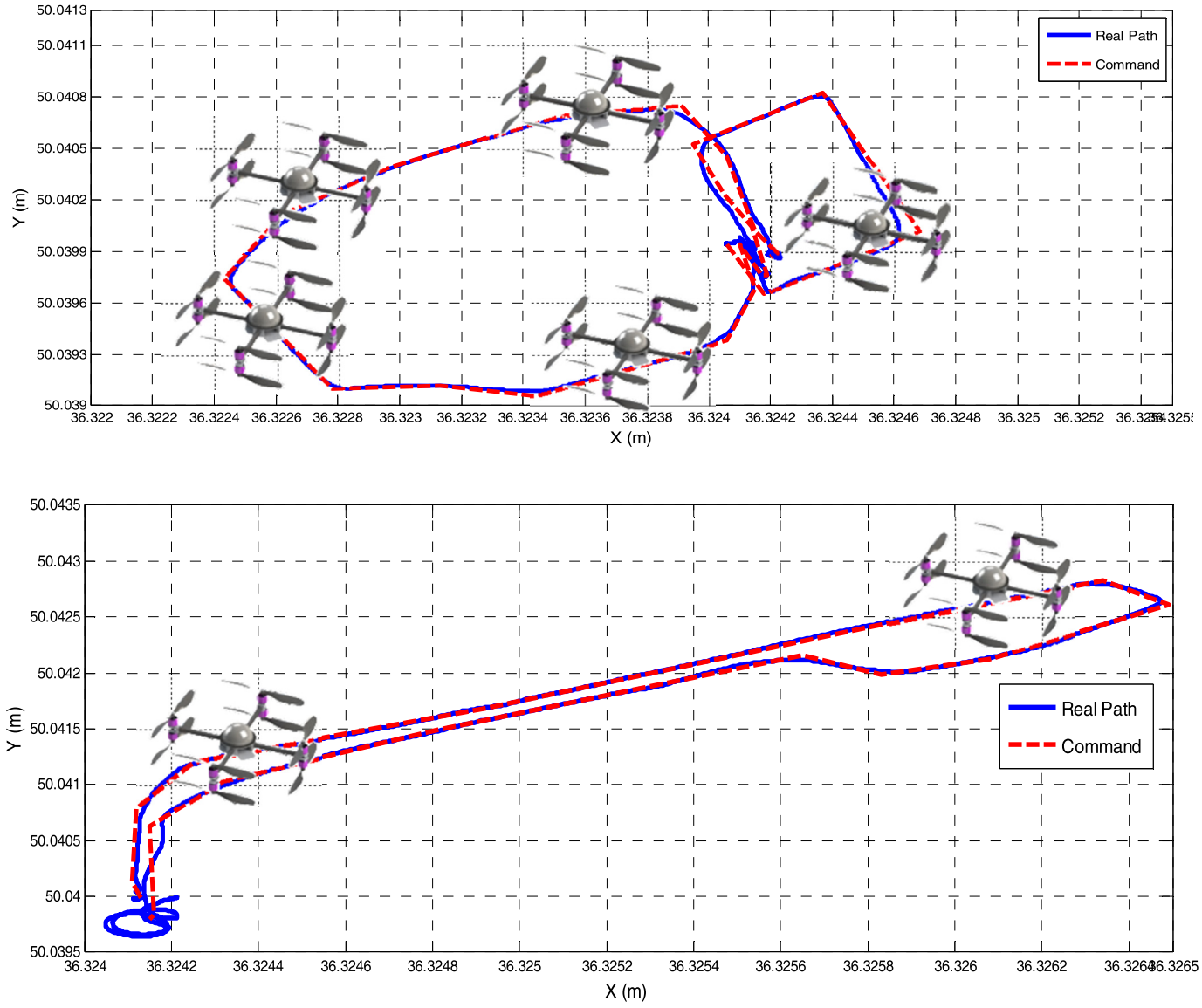

Fig. 13. Path of Octorotor in experiments; (Up) Case study I; (Down) Case study II.

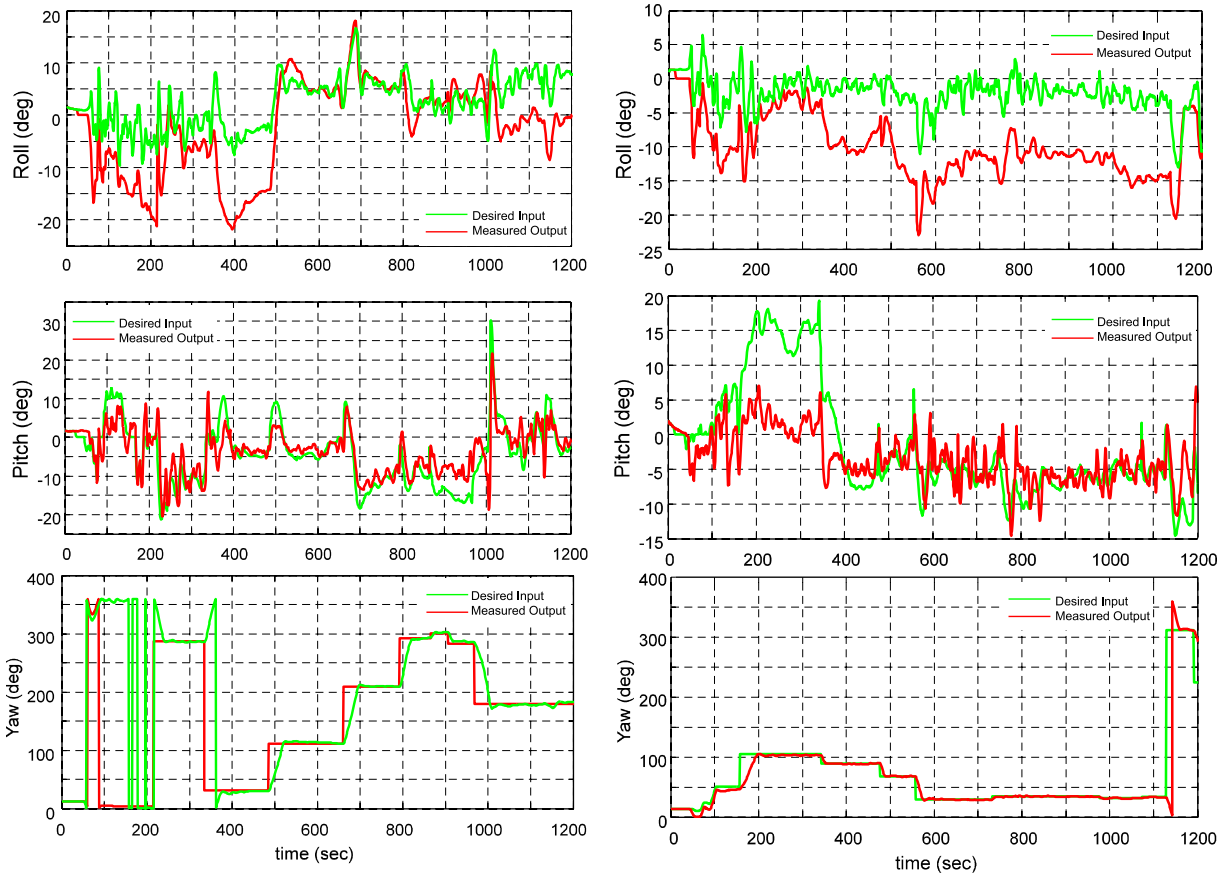

Fig. 14. Euler angles of Octorotor in experiments; (Left) Case study I; (Right) Case study II.

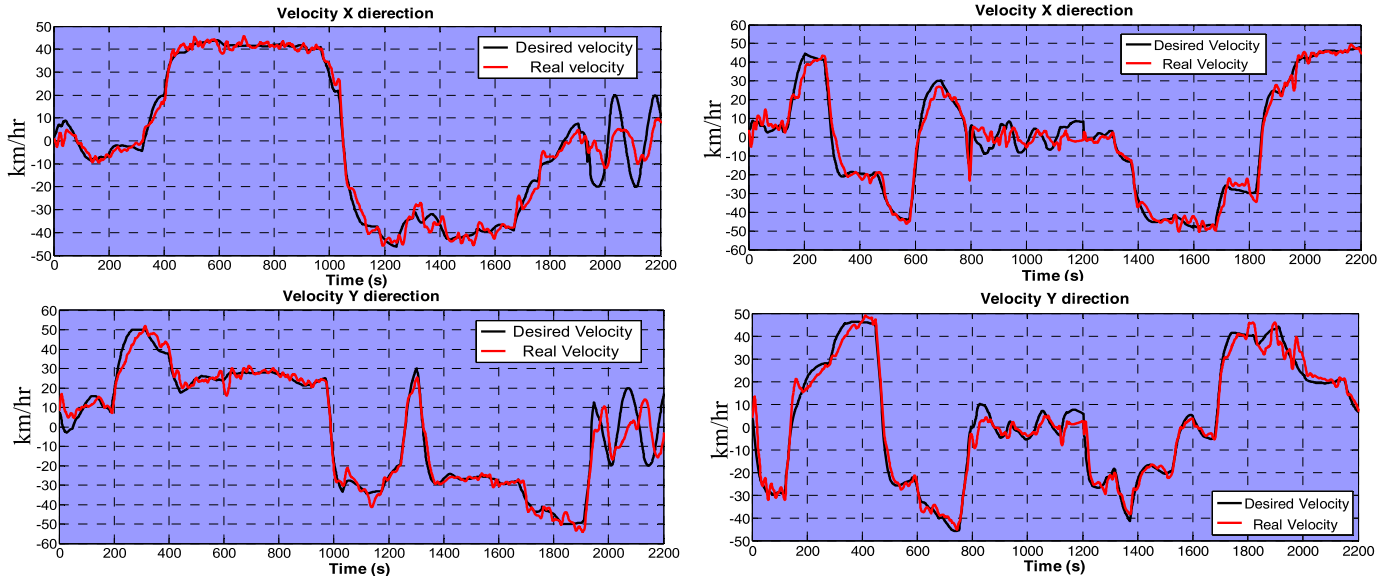

Fig. 15. Linear velocities during the experiments; (Left) first case study; (Right) second case study.

to our previous Quadrotor robot, this Octorotor managed to lift 1.7 times heavier loads. Besides that, in theory, the Octorotor potentially provides tolerance against rotor faults, which will be studied and applied in our future work control design and analysis. Since the rotors are placed coaxially, efficiency loss due to drag interference is less than 7% in different speeds.

Declaration of competing interest

The authors declare the following financial interests/personal relationships which may be considered as potential competing interests: P. Zarafshan reports financial support was provided by Islamic Azad University, Qazvin branch.

Acknowledgement

The authors would like to thank the financial support provided by Islamic Azad University, Qazvin branch for accomplishing this research.

References

[1] P. Zarafshan, S.A.A. Moosavian, M. Bahrami, Comparative controller design of an aerial robot, Aerosp. Sci. Technol. 14 (4) (2010) 276–282.
[2] S.J. Haddadi, P. Zarafshan, Attitude control of an autonomous octorotor, in: 2014 Second RSI/ISM International Conference on Robotics and Mechatronics (ICRoM), IEEE, 2014, pp. 540–545.
[3] P. Pounds, R. Mahony, P. Corke, Modelling and control of a quad-rotor robot, in: Proceedings of the 2006 Australasian Conference on Robotics and Automation, The Australian Robotics and Automation Association Inc., 2006, pp. 1–10.
[4] A. Ebrahimy, P. Zarafshan, S. Hassan-Beygi, M. Dehghani, S. Hashemy, Design and analysis of a solar linear move irrigation system, in: 2018 6th RSI International Conference on Robotics and Mechatronics (IcRoM), IEEE, 2018, pp. 382–387.
[5] F. Hajiahmadi, M. Dehghani, P. Zarafshan, S.A.A. Moosavian, S. Hassan-Beygi, Trajectory control of a robotic carrier for solar power plant cleaning system, in: 2019 7th International Conference on Robotics and Mechatronics (ICRoM), IEEE, 2019, pp. 463–468.
[6] F. Hajiahmadi, P. Zarafshan, M. Dehghani, S.A.A. Moosavian, S. Hassan-Beygi, Dynamics modeling and position control of a robotic carrier for solar panel cleaning system, in: 2019 7th International Conference on Robotics and Mechatronics (ICRoM), IEEE, 2019, pp. 613–618.
[7] P. Pounds, R. Mahony, P. Hynes, J.M. Roberts, Design of a four-rotor aerial robot, in: Proceedings of the 2002 Australasian Conference on Robotics and Automation (ACRA 2002), Australian Robotics & Automation Association, 2002, pp. 145–150.
[8] S. Hanford, L. Long, J. Horn, A small semi-autonomous rotary-wing unmanned air vehicle (UAV), in: Infotech@ Aerospace, 2005, p. 7077.
[9] L.K. Burkamshaw, Towards a Low-Cost Quadrotor Research Platform, Naval Postgraduate School, Monterey, CA, 2010.
[10] K.W. Weng, Design and control of a quad-rotor flying robot for aerial surveillance, in: 2006 4th Student Conference on Research and Development, IEEE, 2006, pp. 173–177.
[11] B. Herisse, F.-X. Russotto, T. Hamel, R. Mahony, Hovering flight and vertical landing control of a VTOL unmanned aerial vehicle using optical flow, in: 2008 IEEE/RSJ International Conference on Intelligent Robots and Systems, IEEE, 2008, pp. 801–806.
[12] B.-C. Min, C.H. Cho, K.M. Choi, D. Kim, Development of a micro quad-rotor UAV for monitoring an indoor environment, in: FIRA RoboWorld Congress, Springer, 2009, pp. 262–271.
[13] D. Liu, H. Liu, J. Xi, Fully distributed adaptive fault-tolerant formation control for octorotors subject to multiple actuator faults, Aerosp. Sci. Technol. 108 (2021) 106366.
[14] E. Baskaya, M. Hamandi, M. Bronz, A. Franchi, A novel robust hexarotor capable of static hovering in presence of propeller failure, IEEE Robot. Autom. Lett. (2021).
[15] P. Zarafshan, S.A.A. Moosavian, E.G. Papadopoulos, Adaptive hybrid suppression control of space free-flying robots with flexible appendages, Robotica 34 (7) (2016) 1464–1485.
[16] H. Zohoor, S.M. Khorsandijou, Dynamic model of a flying manipulator with two highly flexible links, Appl. Math. Model. 32 (10) (2008) 2117–2132.
[17] J.-F. Deü, A.C. Galucio, R. Ohayon, Dynamic responses of flexible-link mechanisms with passive/active damping treatment, Comput. Struct. 86 (3–5) (2008) 258–265.
[18] P. Zarafshan, S.A.A. Moosavian, Cooperative object manipulation by a space robot with flexible appendages, Int. Sch. Res. Not. 2013 (2013).
[19] P. Zarafshan, S.A.A. Moosavian, Dynamics modelling and hybrid suppression control of space robots performing cooperative object manipulation, Commun. Nonlinear Sci. Numer. Simul. 18 (10) (2013) 2807–2824.
[20] P. Zarafshan, S.A.A. Moosavian, Adaptive hybrid suppression control of a wheeled mobile robot with active flexible members, in: 2011 IEEE International Conference on Mechatronics and Automation, IEEE, 2011, pp. 932–937.
[21] K. Rudin, M.-D. Hua, G. Ducard, S. Bouabdallah, A robust attitude controller and its application to quadrotor helicopters, IFAC Proc. Vol. 44 (1) (2011) 10379–10384.
[22] D. Lee, A linear acceleration control for precise trajectory tracking flights of a quadrotor UAV under high-wind environments, Int. J. Aeronaut. Space Sci. (2021) 1–13.
[23] D. Lara Alabazares, A. Rabhi, C. Pegard, F. Torres Garcia, G. Romero Galvan, Quadrotor UAV attitude stabilization using fuzzy robust control, Trans. Inst. Meas. Control (2021) 01423312211002588.
[24] S. Zhou, K. Guo, X. Yu, L. Guo, L. Xie, Fixed-time observer based safety control for a quadrotor UAV, IEEE Trans. Aerosp. Electron. Syst. (2021).
[25] F. Morbidi, D. Pisarski, Practical and accurate generation of energy-optimal trajectories for a planar quadrotor, in: IEEE International Conference on Robotics and Automation, 2021.
[26] D. Cabecinhas, R. Cunha, C. Silvestre, A nonlinear quadrotor trajectory tracking controller with disturbance rejection, Control Eng. Pract. 26 (2014) 1–10.
[27] P. Zarafshan, S.B. Moosavian, S.A.A. Moosavian, M. Bahrami, Optimal control of an aerial robot, in: 2008 IEEE/ASME International Conference on Advanced Intelligent Mechatronics, IEEE, 2008, pp. 1284–1289.
[28] P. Zarafshan, S.A.A. Moosavian, M. Bahrami, Adaptive control of an aerial robot using Lyapunov design, in: 2008 IEEE Conference on Robotics, Automation and Mechatronics, IEEE, 2008, pp. 1–6.
[29] S. Bouabdallah, A. Noth, R. Siegwart, PID vs LQ control techniques applied to an indoor micro quadrotor, in: 2004 IEEE/RSJ International Conference on Intelligent Robots and Systems (IROS) (IEEE Cat. No. 04CH37566), vol. 3, IEEE, 2004, pp. 2451–2456.
[30] Y. Morel, A. Leonessa, Direct adaptive tracking control of quadrotor aerial vehicles, in: ASME International Mechanical Engineering Congress and Exposition, vol. 47683, 2006, pp. 155–161.
[31] N. Kimoto, M. Okochi, N. Matsumoto, T. Nakamaura, Studies of torsional strength of carbon fiber composites shaft by innovative sheet winding, in: Proceedings of the 18th International Conference on Composite Materials, 2011.
[32] H. Desa, S.F. Ahmed, A.Z. Azfar, Adaptive hybrid control algorithm design for attitude stabilization of quadrotor (UAV), Arch. Sci. 66 (2) (2013) 51–64.
[33] M. Dehghani, S.A.A. Moosavian, A new approach for orientation determination, in: 2013 First RSI/ISM International Conference on Robotics and Mechatronics (ICRoM), IEEE, 2013, pp. 20–25.
[34] C. Papachristos, K. Alexis, A. Tzes, Dual–authority thrust–vectoring of a tri–tiltrotor employing model predictive control, J. Intell. Robot. Syst. 81 (3–4) (2016) 471–504.
[35] K. Alexis, C. Papachristos, R. Siegwart, A. Tzes, Robust model predictive flight control of unmanned rotorcrafts, J. Intell. Robot. Syst. 81 (3–4) (2016) 443–469.
[36] S.J. Haddadi, P. Zarafshan, Design and fabrication of an autonomous octorotor flying robot, in: 2015 3rd RSI International Conference on Robotics and Mechatronics (ICROM), IEEE, 2015, pp. 702–707.
[37] S.J. Haddadi, P. Zarafshan, F.J. Niroumand, Dynamics modelling and implementation of an attitude control on an Octorotor, in: 2015 IEEE 28th Canadian Conference on Electrical and Computer Engineering (CCECE), IEEE, 2015, pp. 722–727.